Received: 18 February 2024 | Revised: 20 February 2025 | Accepted: 28 September 2025

DOI: 10.1002/esp.70184

RESEARCH ARTICLE

ESPL WILEY

Formation of repeating bar-flat bedforms in ephemeral gravel bed channels: 2. Bridging mathematical modelling and field observations

Gabriele Massera[1] | Annunziato Siviglia[1] | Jonathan B. Laronne[2,3] | Ian Reid[4] | D. Mark Powell[5] | Tal Cohen[2] | Michael Dorman[6] | Marco Tubino[1]

[1]Department of Civil, Environmental and Mechanical Engineering, University of Trento, Trento, Italy

[2]Department of Earth and Environmental Sciences, Ben Gurion University of the Negev, Beer Sheva, Israel

[3]Dead Sea Arava Science Center, Dead Sea, Israel

[4]Department of Geography and Environment, Loughborough University, Loughborough, UK

[5]Department of Geography, University of Leicester, Leicester, UK

[6]Department of Environmental, Geoinformatics and Urban Planning Sciences, Ben Gurion University of the Negev, Beer Sheva, Israel

Correspondence
Annunziato Siviglia, Department of Civil, Environmental and Mechanical Engineering, University of Trento, Trento, Italy.
Email: annunziato.siviglia@unitn.it

Funding information
Ministero dell'Università e della Ricerca; Israel Science Foundation, Grant/Award Number: 832/14

Abstract

Single- and multi-thread gravel-bed ephemeral channels in semi-arid and arid regions have a characteristic repeating, channel-wide pattern of low angle, fine-grained 'flats' alternating with steeper, coarse-grained 'bars'. The genesis of these macroforms, while a topic of ongoing discussion, has not been fully elucidated. We have documented the formation of these macroforms after both artificially homogenising the bed material of a reach of the Nahal Yatir in the northern Negev, Israel, and ensuring its surface was planar. Here, we integrate the empirical data gained from these field experiments with a novel mathematical model. The model we propose, within a one-dimensional framework, is based on the analysis of flow over an initially planar, erodible bed consisting of a bimodal grain size mixture of sediment. We apply linear stability analysis to derive a solution that provides insight into the formational dynamics of these macroforms. Our results indicate that bar-flat patterns may arise from a free-instability mechanism driven by sediment size heterogeneity, provided that the standard deviation of the sediment grain size distribution (GSD) is sufficiently large. Application of the model to a selection of ephemeral channels of the northern Negev suggests that repeating bar-flat patterns are likely to develop during the recession of flash flood hydrographs, specifically when flow conditions approach the critical threshold for bedload transport. Besides providing a possible explanation for the formation of these macroforms, this study also contributes to a broader understanding of geomorphic processes in dryland river systems.

KEYWORDS
bar-flat bedform, gravel-bed river, linear theory, sediment mixtures, stability analysis

1 | INTRODUCTION

Upland gravel-bed ephemeral streams are characterised by a sequence of repeating macroforms: steep and coarser-grained 'bars' and intervening, almost horizontal, fine-grained 'flats' (Laronne et al., 1994; Powell et al., 2012). These are very clearly visible on the dry channel bed (Figure 1). While several theories have been proposed to explain the formation of macroform sequences in gravel-bed rivers, such as that of pools and riffles (Chin & Wohl, 2005; Church & Zimmermann, 2007; Curran, 2007; Golly et al., 2019; Hassan et al., 2022; Montgomery & Buffington, 1997; Richardson & Carling, 2021), an explanation for the flat-bar sequence has yet to be tested.

High sediment supply has been suggested as the causal factor explaining the lack of armour development in ephemeral channels (Hassan, Egozi, & Parker, 2006; Laronne & Reid, 1993; Reid,

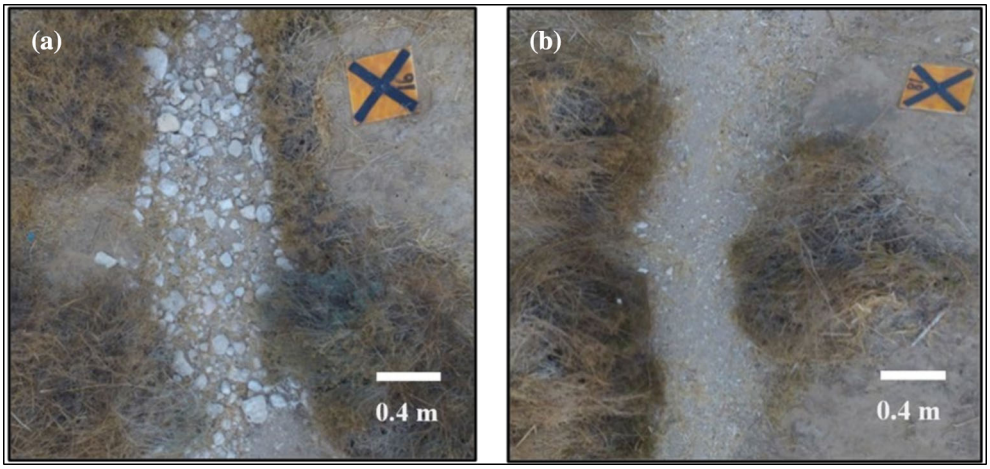

FIGURE 1 Example of a (a) bar unit and a (b) flat unit in the Yatir channel.

Laronne, & Powell, 1995; Stark et al., 2021). However, a hitherto hydraulically untested assertion is that fast hydrograph recession in channels that have a wide range of sediment sizes may explain the alternation of fine- and coarse-grained bedforms in both single- and multi-thread channels (Laronne et al., 1994; Storz-Peretz et al., 2016; Storz-Peretz & Laronne, 2018; Zapico et al., 2018).

We have conducted a series of field experiments, as described in our companion paper (Laronne et al., 2025), to observe whether the flat-bar macroform sequence would be re-established by flash floods after mechanically homogenising the bed material. While these field observations have provided important quantitative insight into the characteristics of the restoration of this sequence, they are not sufficient to elucidate the underlying mechanisms of its formation.

Theoretical approaches are frequently used to fill this kind of knowledge gap. So, for example, stability analysis has been instrumental in explaining the formation of well-sorted sediment macroforms, including ripples, dunes and antidunes (Engelund, 1970; Hayashi, 1970; Kennedy, 1963; Richards, 1980), and the dynamics of fluvial bars under both steady flow conditions (Callander, 1969; Colombini, Seminara, & Tubino, 1987; Parker, 1976) and an unsteady hydrological regime (Carlin, Redolfi, & Tubino, 2021; Redolfi, Carlin, & Tubino, 2023). Here, linear stability analysis will be shown to serve as a useful tool in providing information about the occurrence of bar-flat macroforms and their essential geometric and granulometric characteristics.

Such theoretical tools have been used by others to expand the scope of research to include the impact of sediment-size sorting on bedforms. The focus of these studies has been on understanding how an instability mechanism is influenced by changes in roughness and sediment transport because of the presence of poorly sorted bed material. Noteworthy contributions in this area have come from research on alternate bars (Lanzoni & Tubino, 1999), as well as from investigations designed to understand the formation of bedload sheets (Colombini & Carbonari, 2020; Seminara, Colombini, & Parker, 1996). So, for instance, bedload sheets have been identified as coherent migrating patterns of bed material and have been observed in both flume studies and perennial stream environments to be characterised by units of coarse sand and fine gravel. The phenomenon has been linked intrinsically to the heterogeneous nature of the sediment.

Like bedload sheets, the bar-flat pattern in ephemeral channels displays a recurring sequence of coarse- and fine-grained sediment. However, unlike the uniform bed-surface slope that is characteristic of bedload sheets, the bar-flat pattern is uniquely defined by its alternating segments of near-horizontal, fine-grained flats and steeper, coarse-grained bars (Powell et al., 2012).

The aim of the present study is to identify, by means of a linear approach, the specific conditions that lead to the development of bar-flat sequences in ephemeral streams, as exemplified by those of the northern Negev, Israel. We have demonstrated in a companion paper that a bar-flat sequence that had been obliterated by artificially homogenising and planning the bed material of a channel reach began to reform under successive natural flash floods (Laronne et al., 2025). Here, we show that linear stability analysis can be used to explain the mechanisms by which bars and flats evolve from the same initial conditions, successfully predicting differences in both their surface gradient and their grain size. We also show that it can be used to define the flow conditions during which formation will occur.

2 | FIELD DATA RE-ANALYSIS

Here, we describe the field sites selected for our analysis. This is followed by a detailed assessment of the grain size distributions (GSDs) of the streambed sediments at these sites. Key parameters, including geometric mean and standard deviation of the GSDs, are derived. In addition, we provide hydrometric data collected from the Yatir and Eshtemoa streams. These data are critical to understanding the hydraulic behaviour of the channels, a factor integral to the subsequent modelling analysis and discussion.

2.1 | Field sites and main features of the bar-flat pattern

The field data considered in this study were collected and measured in reaches of the Nahal Yatir, Nahal Eshtemoa and two other neighbouring desert streams of the northern Negev: the Anim and Cryote (Qeriyyot) (Figure 2).

These streams are ephemeral, single-thread, gravel-bed channels that drain the southern flanks of the Judean Highlands, a region of

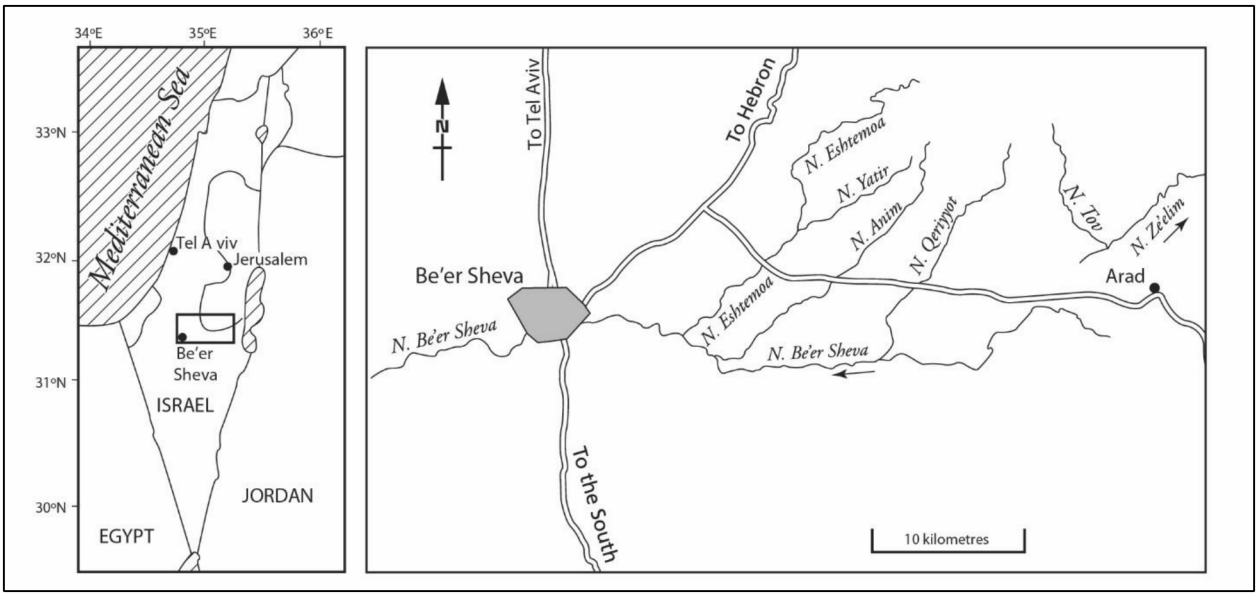

FIGURE 2 Location of the study area (Note: Nahal Cryote is labelled as Nahal Qeriyyot).

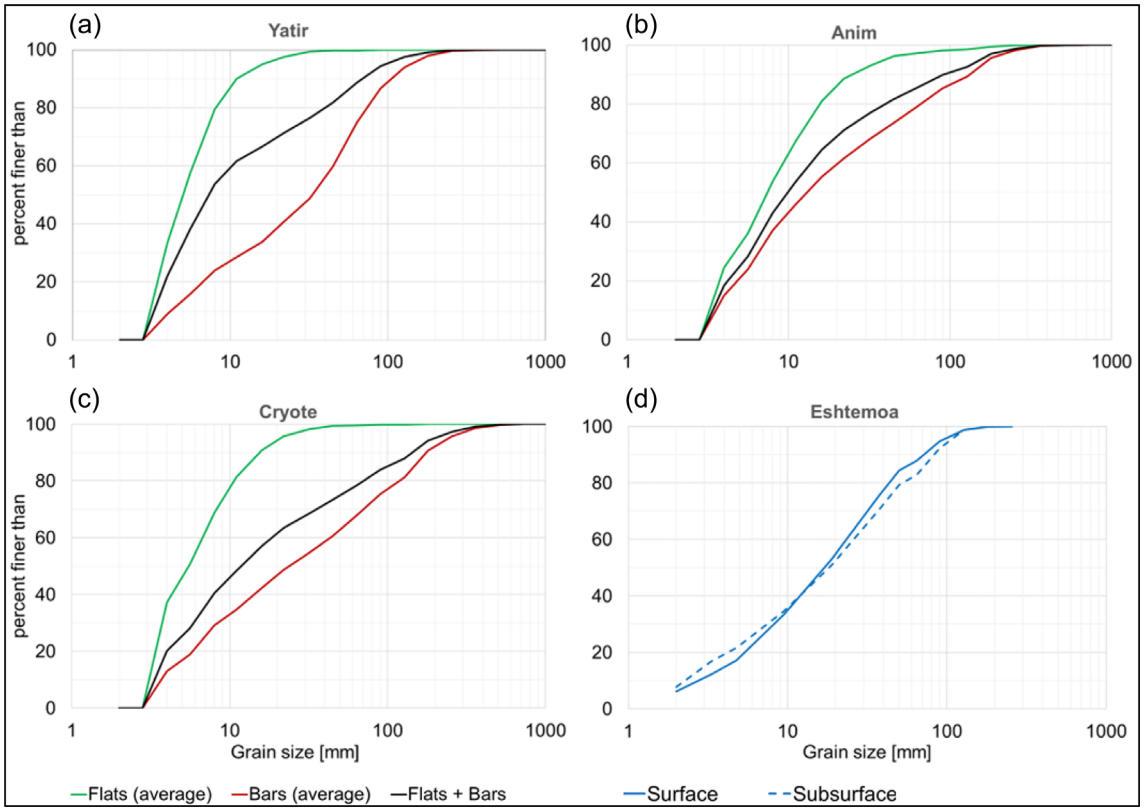

FIGURE 3 Grain size distributions of the ephemeral streams considered in this study.

rolling topography underlain by Upper Cretaceous carbonate rocks (Powell et al., 2012). The streambeds are characterised by a repeating pattern of two dominant units: bars and flats. These units are primarily distinguished by variations in slope, grain size and sediment sorting. Flats are identified as low-gradient units with, variously, positive and negative slopes. In contrast, bars are characterised by consistently steeper slopes, averaging approximately twice the reach-average bed slope. Furthermore, bars exhibit a coarser and less well-sorted sediment composition compared to flats, as described in detail elsewhere (Powell et al., 2012).

2.2 | GSD of the bar-flat pattern

The granulometric dataset used in this study is sourced from the field campaign described in Powell et al. (2012). This dataset includes surface bed material samples from specific reaches of Nahal Yatir, Nahal Anim and Nahal Cryote. The present study also considers the data collected in the Nahal Eshtemoa during the field campaign described in Powell, Reid and Laronne (2001).

Particle size characteristics of several channel units in Nahal Yatir (seven flats and five bars), Nahal Cryote (five flats and five bars) and

Nahal Anim (three flats and four bars) were determined using Wolman counts of sediment > 2 mm diameter (Powell et al., 2012). The sampling registered the number of clasts in grain size classes from 2 to 720 mm for each unit. The resulting aggregate GSDs for these units, obtained by combining all samples, are shown (in black) in Figure 3, with flats and bars differentiated in green and red, respectively, to highlight their particular granulometric characteristics.

A different method was used for Nahal Eshtemoa. Here, large samples of bed material taken from a reach undifferentiated by bars and flats were analysed, resulting in the generation of granulometric curves for both the bed surface and the subsurface (shown as a solid blue line and a dashed blue line, respectively, in Figure 3d). These curves show small differences, indicative of the unarmoured streambeds typical of ephemeral streams in arid zones.

The bed material characteristics of the four channel reaches examined are listed in Table 1. These parameters are fundamental to the mathematical modelling and analysis presented in the following section as they provide a crucial link between empirical data and theoretical interpretation. For the Yatir, the characteristic diameters are comparable to those presented in Table 3 by Cohen (2019) from a more recent field study. Additionally, it is noteworthy that the roughness heights reported in the companion paper for Nahal Yatir (Laronne et al., 2025) are coarser. This inconsistency is attributed to the limitations of the image analysis used in that study, an analysis which, inherently, does not account for the presence of finer-grained sediment fractions.

2.3 | Hydrographs of the Yatir and the Eshtemoa

Several field measurement campaigns have focussed on the hydrological behaviour of ephemeral streams in the northern Negev desert over the last several decades. The earliest studies were conducted on Nahal Yatir in 1989–90, with results documented in Laronne and Duncan (1992) and Reid, Laronne and Powell (1995). Additionally, Reid, Laronne and Powell (1998) analysed the hydrographs of Nahal Eshtemoa during the four rain seasons of 1991 through 1995. In the present study, we have used an up-to-date hydraulic dataset, specifically that of January 2018 for the Yatir and that from January 2017 through 2018 for the Eshtemoa.

Figure 4a shows five hydrographs from Nahal Yatir. The labels attached to the flood events, T7 through T10, reflect those used in the companion paper (Laronne et al., 2025). The only difference is that T9 is divided into a pair of sub-events, T9a and T9b, as they are considered to represent two distinct floods. Water stage was monitored using a Levelogger 5 (Solinst) equipped with a non-vented pressure sensor having a full-scale accuracy of ±0.05%. Water depth was established after compensating for changes in atmospheric pressure (Laronne et al., 2025). The hydrographs exhibit a bore-like, rapid rise in water level followed by a more gradual recession, common characteristics of flow events in ephemeral streams of the northern Negev. Three hydrographs recorded in the 2017 and 2018 winter seasons in Nahal Eshtemoa have also been used (Figure 4b). These were recorded using vented pressure transducers (Druck PTX 1730,

TABLE 1 Bed material characteristics of the four study reaches derived from the respective grain-size distribution curves: D_{g0} is the overall geometric mean diameter of the distribution, σ_g is the geometric standard deviation and σ_0 is the standard deviation of the distribution; $D_{g,\text{bars}}$ and $D_{g,\text{flats}}$ represent the geometric mean diameters of grains in bars and flats, respectively.

		Nahal Yatir	Nahal Eshtemoa	Nahal Anim	Nahal Cryote
D_{g0}	[mm]	11	15	15	13
σ_g	[–]	3.13	3.26	3.46	4.24
σ_0	[–]	1.69	1.71	1.79	2.10
$D_{g,\text{bars}}$	[mm]	25.4	-	16.9	24.3
$D_{g,\text{flats}}$	[mm]	5.5	-	8.0	5.7

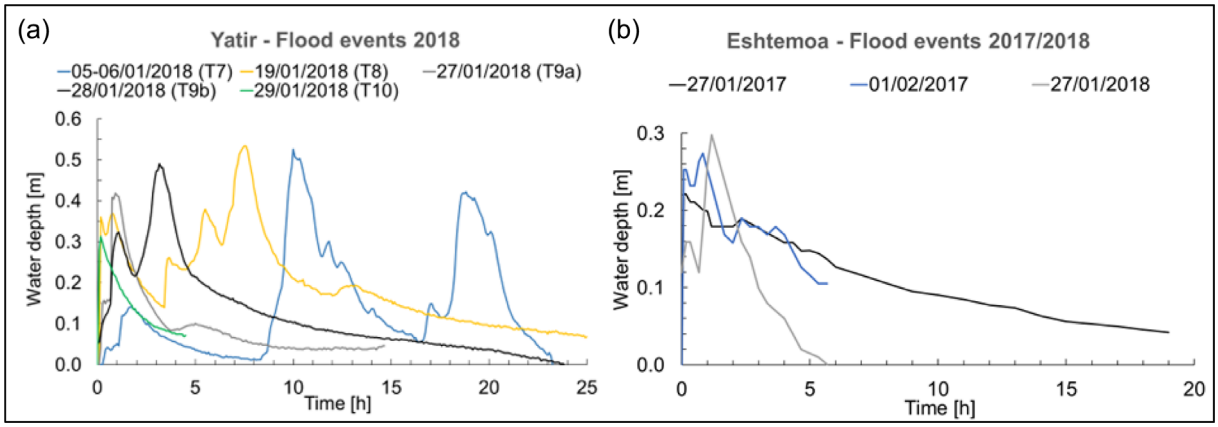

FIGURE 4 (a) Nahal Yatir flood hydrographs during the winter season 2018 and (b) Nahal Eshtemoa flood hydrographs during the 2017 and 2018 winter seasons. In comparison with the hydrographs presented in the companion paper, the event of 19 January 2018 is truncated here after 25 h, while that of 29 January 2018 is truncated after 5 h. The Eshtemoa hydrograph of 01 February 2017 ends abruptly above a depth of 10 cm because high concentrations of suspended solids led to clogging of the stilling wells, thereby impairing the record. Dates in the image are in day/month/year format.

±0.25% accuracy). They also demonstrate the distinctive rapid rise and longer fall in water levels.

3 | MATHEMATICAL MODEL

In this section, we describe the mathematical model that we have used to analyse the probable formation of bar-flat patterns. The formulation follows closely that proposed by Lanzoni and Tubino (1999) to investigate the effect of sediment heterogeneity on the development of alternate bars. However, a simplified, one-dimensional approach is adopted here, which is justified by the dominant longitudinal character of the phenomenon under investigation. The model is based on the solution of the steady Saint–Venant flow equations and the Exner sediment continuity equation for each grain-size fraction, coupled with a suitable model for the transport of a sediment mixture, where Hirano's (1971) concept of the active layer is adopted.

3.1 | Formulation of the problem

For present purposes, we consider a straight channel with non-erodible banks and constant width, the bed of which is composed of a mixture of cohesionless sediment. We denote by $f(\phi)$ the probability density function of grain sizes in the mixture, where ϕ is the sedimentological, base-2 logarithmic scale for particle size, namely $\phi = -\log_2(D_s)$, with D_s sediment diameter (in mm). We assume that the distribution of grain sizes can change both in the longitudinal direction (x^*) and in time (t^*)[1], while it is constant in the vertical direction, as we do not expect significant effects of vertical sorting because of the low relief of the bar-flat pattern. Notably, field observations (Laronne et al., 1994) indicate the absence of an armour layer.

The objective of our study is to determine the response of the flow field and sediment transport to perturbations of the bed elevation and GSD by varying the reach-averaged flow conditions. These conditions are defined, for a given value of unit water discharge, in terms of the water depth D_0^* and velocity U_0^* of the uniform flow over a flat bed with constant slope S_0 and a longitudinally well-mixed, cohesionless sediment with GSD $f_0(\phi)$. We then use the above average quantities to set the governing equations in the following dimensionless form:

$$U\frac{\partial U}{\partial x} + Fr_0^{-2}\left(\frac{\partial D}{\partial x} + \frac{\partial \eta}{\partial x}\right) + C_f\frac{U^2}{D} = 0, \tag{1}$$

$$\frac{\partial (UD)}{\partial x} = 0, \tag{2}$$

$$f\frac{\partial \eta}{\partial t} + L_a\frac{\partial f}{\partial t} + \frac{\partial (fq_s)}{\partial x} = 0, \tag{3}$$

where U is the longitudinal velocity, D the water depth, η the bed elevation, and the product fq_s is the volume of bedload transport rate per unit width of a grain size fraction. Furthermore, Fr_0 is the Froude number of the average uniform flow, C_f the friction coefficient, and L_a the thickness of the active surface layer.

The system (1–3) is complemented by the overall mass balance equation for the sediment mixture, which is obtained by integrating Equation (3) over the grain sizes:

$$\frac{\partial \eta}{\partial t} + \int_{-\infty}^{\infty} q_s\frac{\partial f}{\partial x}\,d\phi + \int_{-\infty}^{\infty} f\frac{\partial q_s}{\partial x}\,d\phi = 0. \tag{4}$$

In Equations (1–4), variables have been made dimensionless through the following scaling:

$$U = \frac{U^*}{U_0^*}, \quad (D, \eta, x, L_a) = \frac{(D^*, \eta^*, x^*, L_a^*)}{D_0^*}, \quad t = \frac{t^* q_0}{\left[(1-p)D_0^{*2}\right]}, \quad q_s = \frac{q_s^*}{q_0}, \tag{5}$$

where

$$q_0 = \sqrt{\Delta g {D_{g0}}^3}, \quad \Delta = \left(\frac{\rho_s}{\rho} - 1\right), \tag{6}$$

and p is sediment porosity, g is gravitational acceleration, ρ and ρ_s denote fluid and sediment density, respectively, and D_{g0} is the geometric mean diameter of the sediment mixture.

To solve the mathematical problem defined by Equations (1–4) for the unknown variables (U, D, η, f), suitable closure relations are required to compute the friction coefficient and the bedload flux. The friction coefficient C_f is expressed in terms of the local relative roughness through the logarithmic formula (Keulegan, 1938; Parker, 1992):

$$C_f = \left[6 + 2.5\ln\left(\frac{D^*}{k_s}\right)\right]^{-2}, \quad k_s = nD_\sigma, \tag{7}$$

where the constant n is usually assigned in the range $(2-2.5)$, and $D_\sigma = D_g\sigma_g$ is a grain size representative of the coarser fraction, which depends on the parameters of the local bed composition, namely the geometric mean diameter D_g and the standard deviation σ_g. They are defined in terms of the first and the second moment of the local GSD $f(\phi)$ in the form:

$$D_g = 2^{-\overline{\phi}}, \quad \sigma_g = 2^{\sigma}, \tag{8}$$

where

$$\overline{\phi} = \int_{-\infty}^{\infty} f\,\phi\,d\phi, \quad \sigma^2 = \int_{-\infty}^{\infty} f\,(\phi - \overline{\phi})^2\,d\phi. \tag{9}$$

The bedload function q_s is expressed through the following relationship:

$$q_s = {\theta_g}^{3/2}\,G(\zeta), \tag{10}$$

where θ_g is the Shields parameter associated with the geometric mean diameter D_{g0}, namely

[1]Here and in the following, the * asterisk denotes dimensional variables that are subsequently made dimensionless.

$$\theta_g = \frac{{u_*}^2}{\Delta g D_{g0}}, \tag{11}$$

in which $u_* = \sqrt{C_f} U^*$ is the friction velocity, and $G(\zeta)$ is the transport capacity function. Among the various empirical transport predictors available in the literature, the Parker (1979) formulation is adopted here:

$$G(\zeta) = 11.2\left(1-\frac{1}{\zeta}\right)^{4.5}, \quad \zeta = \frac{\theta_g}{\theta_c}\frac{D_{g0}}{D_g} g_{hr}\left(\frac{D_s}{D_g}\right), \quad g_{hr} = \left(\frac{D_s}{D_g}\right)^{-b}, \tag{12}$$

where $\theta_c = 0.03$ is the critical Shields parameter for sediment motion. The reduced hiding function g_{hr} accounts for the effect of the different mobilities of grain sizes in the mixture. Based on the calibration performed for Nahal Yatir by Powell, Reid, and Laronne (2001) and Powell, Laronne and Reid (2003), a value of $b = 0.26$ is set here.

Finally, the thickness of the active layer L_a^* is taken as equal to the local roughness height k_s.

3.2 | Linear stability analysis

The system described by Equations (1–4), and supplemented by the closure relations (7) and (10), provides a steady uniform solution for the flow of water and sediment transport for any specified combination of unit water discharge, bed slope and bed material characteristics. Hereafter, we refer to this solution as the 'reference state' and use the subscript '0' to denote the corresponding variables.

We note that such a reference state is defined, in dimensionless form, once the values of the Shields parameter (θ_{g0}) and of grain ratio (d_{g0}) are given, namely

$$\theta_{g0} = \frac{S_0 D_0^*}{\Delta g D_{g0}}, \quad d_{g0} = \frac{D_{g0}}{D_0^*}, \tag{13}$$

and the standard deviation σ_0 of the GSD $f_0(\phi)$ is specified.

We proceed by employing a linear analysis to assess the stability of the reference state in response to perturbations in both the bed-surface configuration and the GSD. Our approach involves tracking the temporal evolution of small-amplitude sinusoidal perturbations initially applied to the reference state's bed elevation and GSD. Of note is that a periodic variation of bed elevation entails an alternation of steeper and less steep segments.

To carry out this analysis, we express the unknown variables in the following form:

$$(U, D, \eta, f) = [1, 1, \eta_0(x), f_0(\phi)] + \varepsilon[U_1(x,t), D_1(x,t), \eta_1(x,t), f_1(\phi; x, t)] + O(\varepsilon^2), \tag{14}$$

where $\varepsilon \ll 1$ is a small parameter and η_0 is the unperturbed bed elevation, that is, $-(d\eta_0/dx) = S_0$.

Using the closure relationships (7) and (10), a similar expansion is obtained for the friction coefficient and the following bedload function

$$C_f = C_{f0}(1 + \varepsilon C_{f1}) + O(\varepsilon^2), \quad q_s = q_{s0}(1 + \varepsilon q_{s1}) + O(\varepsilon^2), \tag{15}$$

where C_{f0} and q_{s0} denote the friction coefficient and the bedload function of the reference state.

On substituting from (14) into the governing Equations (1–4) and neglecting higher-order terms, we obtain a linear differential system for the unknown variables (U_1, D_1, η_1, f_1), the solution of which is sought through a normal mode analysis (the mathematical procedure to derive the linear system is reported in Appendix A). The solution for the perturbations can be given in the following complex form:

$$(\eta_1, U_1, D_1, f_1) = \left[\widehat{\eta}_1(t), \widehat{U}_1(t), \widehat{D}_1(t), \widehat{f}_1(t)\right] \exp(i\alpha x) + c.c.\,, \tag{16}$$

where α is the dimensionless wavenumber of the perturbations, $\left(\widehat{\eta}_1, \widehat{U}_1, \widehat{D}_1, \widehat{f}_1\right)$ are complex functions that define the amplitude and phase of each variable, and c.c. denotes the complex conjugate. The structure of the solution (16) for the perturbation of bed elevation implies a sinusoidal variation of the local bed slope:

$$S = S_0 + \varepsilon S_1, \quad S_1 = -(\partial\eta_1/\partial x) = -i\alpha\widehat{\eta}_1 \exp(i\alpha x) + c.c.\,, \tag{17}$$

which represents an alternation of steeper and less steep segments.

The functions (η_1, f_1) represent periodic oscillations in the longitudinal direction between positive and negative values of the perturbations of bed elevation (i.e. of local bed slope) and grain size. Furthermore, the complex nature of the amplitude functions $\left(\widehat{\eta}_1, \widehat{f}_1\right)$ implies that the linear solution takes into account the possible phase shift of the longitudinal variation of bed material composition with respect to that of the bed profile.

In the following, we consider the simplest solution of the linear problem—namely, that corresponding to a bimodal mixture composed of two discrete grain sizes: a coarser (C) and a finer (F) fraction. The analysis can, however, be readily generalized to account for a larger number of fractions. In this case, the GSD can be expressed as

$$f(\phi) = (f_{C0} + \varepsilon f_{C1})\,\delta(\phi - \phi_C) + (f_{F0} + \varepsilon f_{F1})\,\delta(\phi - \phi_F), \tag{18}$$

where δ is the Dirac function. The GSD must satisfy the integral condition

$$\int_{-\infty}^{\infty} f\, d\phi = \int_{-\infty}^{\infty} (f_0 + \varepsilon f_1) d\phi = 1, \tag{19}$$

which implies that $f_{F0} = (1 - f_{C0})$ and $f_{F1} = -f_{C1}$. Therefore, in the case of a bimodal mixture, the unknown distribution f_1 can be replaced by f_{C1}.

Details of the mathematical procedure for solving the linear problem are given in Appendix B. It is sufficient to recall that, using Equation (16), the linearized flow equations reduce to an algebraic system, which allows us to express the unknown variables $\left(\widehat{U}_1, \widehat{D}_1\right)$ in terms of $\left(\widehat{\eta}_1, \widehat{f}_{C1}\right)$. Upon substituting into the linearised form of mass balance Equations (3) and (4), we derive a system of two linear differential equations governing the temporal evolution of the perturbations of bed elevation and GSD, which takes the following form:

$$\frac{d\widehat{f}_{C1}}{dt}=\Psi_{11}\widehat{f}_{C1}+\Psi_{12}\widehat{\eta}_1,\qquad \frac{d\widehat{\eta}_1}{dt}=\Psi_{21}\widehat{f}_{C1}+\Psi_{22}\widehat{\eta}_1, \tag{20}$$

where the complex coefficients $\Psi_{kj}\,(k=1,2;j=1,2)$ depend on the parameters of the reference flow $(\theta_{g0},d_{g0},\sigma_0)$. The system (20) poses an eigenvalue problem, which admits solutions that are exponentially dependent on time:

$$\begin{aligned}\left(\widehat{\eta}_1,\widehat{f}_{C1}\right)=&\left(\widehat{\eta}_{1+},\widehat{f}_{C1+}\right)\exp[(\Omega_+-i\omega_+)t]\\&+\left(\widehat{\eta}_{1-},\widehat{f}_{C1-}\right)\exp[(\Omega_--i\omega_-)t],\end{aligned} \tag{21}$$

where $\Omega_\pm$ and $\omega_\pm$ are the growth rate and the angular frequency of perturbations, obtained through the following dispersion relation:

$$(\Omega_\pm-i\omega_\pm)=\frac{1}{2}\left[(\Psi_{11}+\Psi_{22})\pm\sqrt{(\Psi_{11}-\Psi_{22})^2+4\Psi_{12}\Psi_{21}}\right]. \tag{22}$$

When the perturbation of the GSD is neglected, that is, $\widehat{f}_{C1}$ vanishes, the resulting eigenvalue has a negative growth rate. This implies that, in the absence of sediment heterogeneity, the one-dimensional model always predicts stability of the flat bed configuration.

4 | RESULTS

4.1 | Results of stability analysis

The dispersion relationship (22) represents the main outcome of the linear stability theory. A negative value of the growth rate implies that the initial perturbations decay over time and the reference state is stable, while a positive value means that perturbations of bed slope and bed composition can grow, leading to the formation of a bar-flat pattern, with an associated alternation of steeper, coarser patches and finer-grained, less steep patches.

The homogeneous character of the governing system (20) highlights the free nature of the instability mechanism here investigated. The bar-flat pattern arises spontaneously, without the influence of external factors, such as channel curvature or width variations. The initial small-amplitude perturbations in bed elevation and GSDs drive linear perturbations in bed stress and sediment transport, which in turn control the temporal evolution of bars and flats.

In the case of a bimodal mixture, for a given set of the parameters of the reference state $(\theta_{g0},d_{g0},\sigma_0)$ and for any value of the wavenumber of the perturbations α, we obtain two different values of Ω. One of these (Ω_-) is invariably negative and coincides, as σ_0 vanishes, with that of the uniform sediment case. The other (Ω_+), obtained from (22) by choosing the positive root, is inherently associated with the heterogeneous character of the sediment; its value mainly depends on the standard deviation σ_0 of the sediment mixture. Specifically, the value of Ω_+ turns from negative to positive as σ_0 increases, within a range of values of the Shields stress above the critical threshold that widens with σ_0.

An example of a stability diagram is represented in Figure 5a, where the growth rate Ω_+ is reported on the $(\theta_{g0}/\theta_c,\ \sigma_0)$ parameter space, for a given value of the grain ratio d_{g0}. The results shown in Figure 5a are obtained with an initial balanced composition of the mixture, that is, $f_{C0}=f_{F0}=0.5$, and a dimensionless wavenumber of the perturbations $\alpha=0.02$. This value has been selected on the basis of the observed longitudinal spacing of bar-flat sequences (Powell et al., 2012), which is in the range of $30-70$ m, while the water depth is in the order of a few decimetres, which implies that typical values of α are in the range $0.01-0.04$.

Figure 5a highlights the existence of three distinct regions on the $(\theta_{g0}/\theta_c,\ \sigma_0)$ parameter space. For relatively low values of the standard deviation of the mixture σ_0, the growth rate Ω_+ is negative (Stability region) and the unform flow and transport of the sediment mixture is stable. When the standard deviation exceeds a threshold value ranging between 1.4 and 1.5, a region appears where the growth rate Ω_+ is positive (Instability region), and therefore, perturbations of bed slope and bed composition can grow. The instability region is bounded

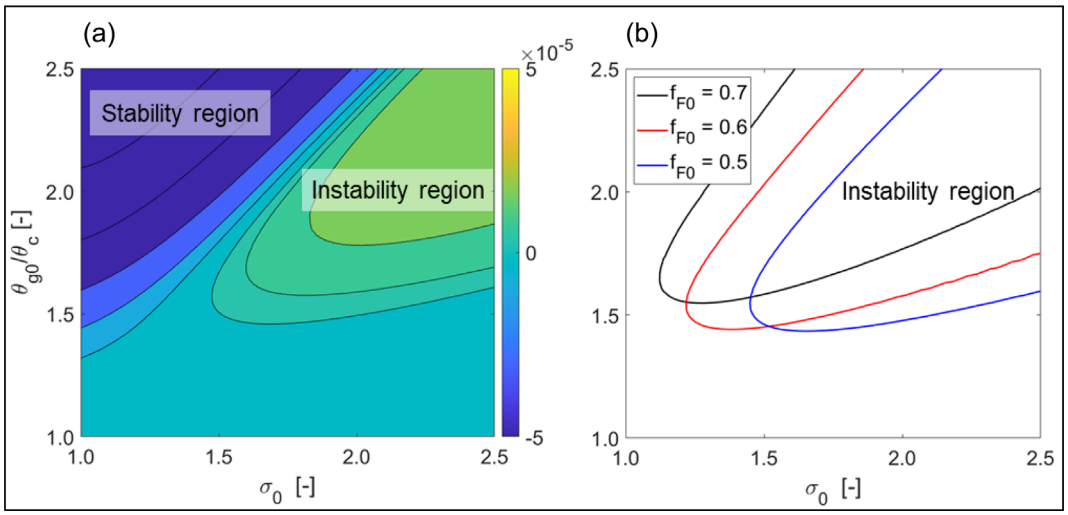

FIGURE 5 Stability diagram for bar-flat patterns on the $(\theta_{g0}/\theta_c,\ \sigma_0)$ plane, for a given value of the grain ratio $d_{g0}=0.01$ and $\alpha=0.02$: (a) contour plot of the growth rate Ω_+ of bar-flat patterns (the growth rate is negative in the blue-to-dark blue area, positive in the light-green-to-green area, and vanishes in the homogeneous turquoise area); (b) the marginal curves delimiting the instability region where the linear theory predicts the occurrence of bar-flat patterns for different values of the finer fraction f_{F0} in the sediment mixture.

by an upper value of the ratio θ_{g0}/θ_c that increases as σ_0 increases, and by a lower value that keeps it in the range $1.4-1.6$. The latter value corresponds to the critical threshold for the sediment motion of the coarse fraction within the mixture. Below this value, a condition of partial transport occurs, because only the fine fractions are transported, and the growth rate Ω_+ vanishes.

The above scenario does not change by varying the grain-size ratio within the range of values that is typical of gravel-bed rivers, the lower and upper limits of the instability region being almost independent of d_{g0}. Therefore, the linear stability analysis invariably predicts the possible formation of a periodic variation of bed slope and bed composition when the standard deviation of the sediment mixture is sufficiently large, and the Shields parameter remains close to θ_c. The region of possible formation of a bar-flat pattern considerably widens when increasing the finer fraction f_{F0} of the mixture of sediments, as shown in Figure 5b.

The linear stability theory, being restricted to infinitesimal perturbations ($\varepsilon \ll 1$), is obviously unable to yield information on the final amplitude of perturbations. However, from the linear solution, it is possible to compute the spatial distribution of local bed composition for a given distribution of bed elevation. Indeed, such information is crucial to being able to understand whether the theory is capable of correctly reproducing the phenomenon under investigation, namely the concurrence of steeper, coarser-grained channel-bed segments and less steep, finer-textured segments.

As pointed out above, the functions (η_1, f_{C1}) represent sinusoidal variations in the longitudinal direction of the perturbations of bed elevation and of the coarse fraction. Specifically, a positive (negative) value of f_{C1} expresses a local excess (defect) of the coarse fraction in the bed material composition with respect to the average composition of the sediment mixture. To compute the phase shift of the longitudinal variation of the coarse fraction with respect to that of bed profile, we take advantage of the homogeneous character of system (20), which implies that, by substituting the solution (21), we obtain two linearly dependent equations. Thus, either of the equations can be used to derive the relationship between the complex amplitudes $\left(\widehat{\eta}_1, \widehat{f}_{C1}\right)$. Considering the first term of the solution (21), we find that, within the range of values of parameters corresponding to the instability region ($\Omega_+ > 0$), the phase shift is almost constant and the function f_{C1} has its maximum positive value (i.e. the maximum local excess of the coarse fraction) at about a quarter of the wavelength downstream with respect to the peak of the bed profile. This is shown in Figure 6a, where a value of the standard deviation typical of the ephemeral streams of the northern Negev ($\sigma_0 = 1.7$) is used. Recalling Equation (17), this implies that the perturbation of the coarse fraction is nearly in phase with the perturbation of the bed slope.

Therefore, the linear solution predicts that the bed is coarser where the bed slope is steeper (i.e. on bars), while it is finer-grained where the slope is less steep (i.e. on flats). Furthermore, Figure 6b suggests that, within the instability region, the amplitudes of the perturbations of bed elevation and of bed material composition are of the same order of magnitude.

4.2 | Application to the ephemeral northern Negev channels

The results of linear stability theory demonstrate that bar-flat patterns may arise from an inherent free-instability mechanism driven by sediment heterogeneity when the standard deviation of the sediment mixture is sufficiently large and the hydrodynamic conditions are not far above the critical threshold for bedload transport.

TABLE 2 Input parameters for the stability analysis.

		Nahal Yatir	Nahal Eshtemoa
ρ	[kg/m^3]	1,040	1,022
ρ_s	[kg/m^3]	2650	2650
S_0	[−]	0.0087	0.0075
d_{g0}	[−]	0.05	0.1

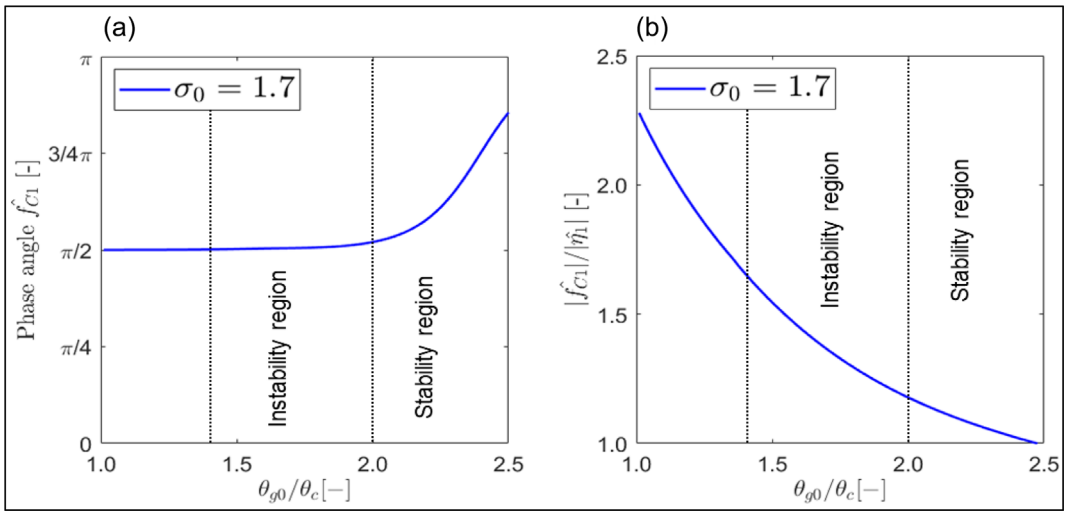

FIGURE 6 The dependence on the ratio θ_{g0}/θ_c of the (a) phase angle and of the (b) amplitude of the longitudinal oscillation of the coarse fraction $\left(\widehat{f}_{C1}\right)$ with respect to those of the longitudinal oscillation of the bed profile, for given values of the grain ratio $d_{g0} = 0.01$ and of the standard deviation $\sigma_0 = 1.7$, and $\alpha = 0.02$. The phase angle is expressed in radians: a phase angle equal to $\pi/2$ implies that the coarse fraction peaks at a quarter of a wavelength downstream of the maximum of bed elevation.

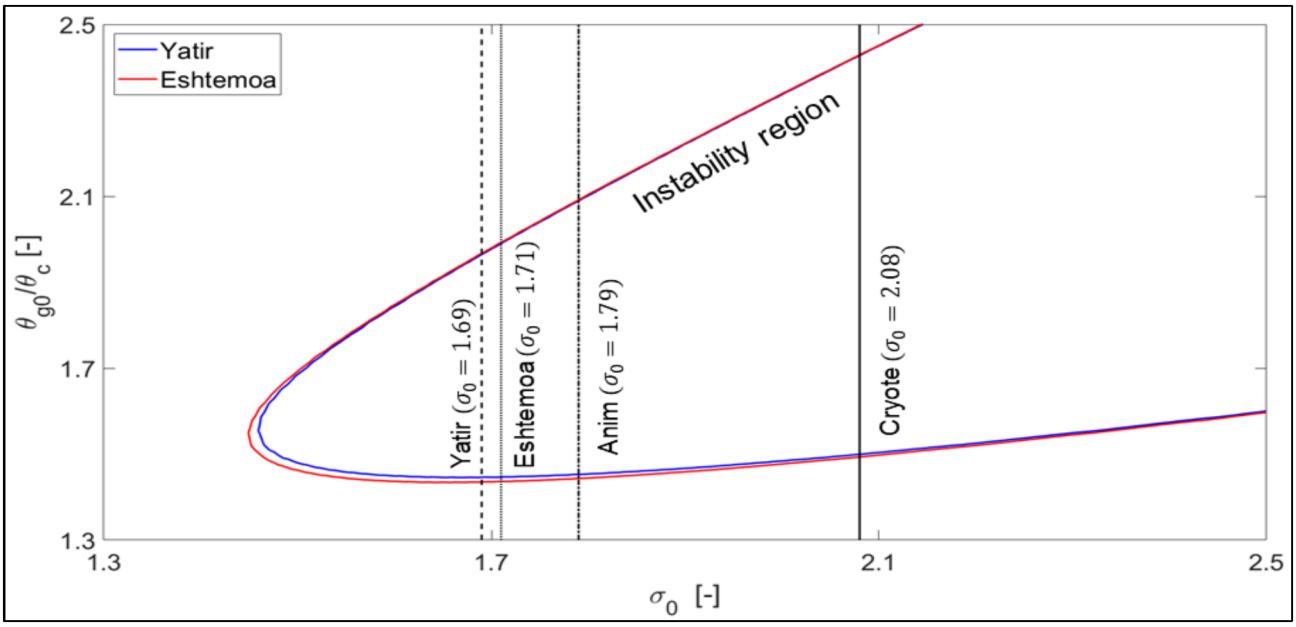

FIGURE 7 The marginal curves delimiting the region on the $(\theta_{g0}/\theta_c,\ \sigma_0)$ plane where bar-flat patterns are developed, as predicted by the linear theory with $d_{g0} = 0.05$ (Yatir, blue line) and $d_{g0} = 0.1$ (Eshtemoa, red line), and the values of the standard deviation σ_0 of the bed material GSD of four ephemeral northern Negev channels.

We now test whether these theoretical findings can provide a possible explanation for the formation of such repeating forms in the ephemeral channels of the northern Negev described in the companion paper (Laronne et al., 2025). The bed material characteristics of the four study reaches are reported in Table 1. Further parameters for Nahal Yatir and Nahal Eshtemoa, for which water stage measurements are also available, are presented in Table 2, where d_{g0} has been computed using a representative mean value of the water depth D_0^*.

In Figure 7, the values of the standard deviation of the GSD measured in the four study reaches (see Table 1) are reported on the stability diagram in the $(\theta_{g0}/\theta_c,\ \sigma_0)$ plane, together with the marginal curves corresponding to two different values of the grain ratio, $d_{g0} = 0.05$ and $d_{g0} = 0.1$, that are representative of Nahal Yatir and Nahal Eshtemoa, respectively. Because the contour of the instability region is almost independent of d_{g0}, either curve can be taken as fairly representative of the other two study reaches (Nahal Anim, Nahal Cryote). Figure 7 shows that, in all four cases examined, the standard deviation σ_0 is larger than the threshold value, which implies that there is a range of θ_{g0}/θ_c values, that is, of flow conditions, that promotes the formation of bar-flat patterns. Specifically, the region of instability occurs when θ_{g0}/θ_c falls in the range $1.44 - 1.96$, for Nahal Yatir, and in the similar range $1.44 - 2.0$, for Nahal Eshtemoa, while a slightly wider range of instability is predicted for Nahal Anim and a much wider range for Nahal Cryote, as they exhibit larger values of σ_0.

The instability ranges given above can be converted into the equivalent ranges of water depth once a suitable estimate of flow depth D_{0c}^* corresponding to incipient sediment motion is given. A first estimate is obtained from Equation (13), setting $\theta_{g0} = \theta_c = 0.03$, which results in $D_{0c}^* = 0.063\,m$ for the Nahal Yatir and $D_{0c}^* = 0.10\,m$ for the Nahal Eshtemoa. Reid, Laronne and Powell (1998) suggest for both ephemeral streams a similar value of the critical depth ($D_{0c}^* \cong 0.10\,m$). The resulting range of water depths that promote the formation of bar-flat patterns in Nahal Yatir is equal to $0.09 - 0.12\,m$, with the former estimate of D_{0c}^*, and equal to $0.14 - 0.20\,m$, with the latter. The same range of water depths is obtained for Nahal Esthemoa.

A glance at the hydrographs of Nahal Yatir and Natal Eshtemoa (Figure 4) suggests that these conditions can last several hours during flow recession typical of these ephemeral streams. Computing for each flood event the duration of flow states during recessions that fall within the instability region, we obtain the results reported in Figure 8. It appears that the formative conditions of bar-flat patterns predicted by linear stability theory correspond, on average, to about $25 - 30\%$ of the total duration of the recessions in the Nahal Yatir and 50% in the Nahal Eshtemoa. Furthermore, the duration of formative conditions varies between 1 and 5 h.

The linear theory also predicts that, under unstable conditions, the perturbation of the GSD is such as to produce grain size coarsening of steeper units, that is, bars, and grain size fining in areas of less steep slope, with the amplitude of the bed material composition perturbation having the same order of magnitude as that of bed elevation (Figure 6b). The field observations made in Nahal Yatir and reported in our companion paper (Laronne et al., 2025) provide support for the outcome of the theoretical analysis. Computing the mean value of the differences in local longitudinal slope between bars and flats from the data shown in Table 3 of Laronne et al. (2025) and using Equation (17), we obtain $\varepsilon|\hat{\eta}_1| \cong 0.12$. A similar estimate results from the distribution of heights derived from digital elevation models reported in Table 2S of Laronne et al. (2025), where the values corresponding to the 95th percentile of bars and to the 5th percentile of flats have been used to estimate the maximum and minimum bed elevation, respectively. Using Equation (18) and the graph reported in Figure 6b to evaluate the ratio $|\hat{f}_{C1}|/|\hat{\eta}_1|$, we then obtain an estimate of the coarse fraction of bars, $f_{C,bars}$, ranging between 0.79 and 0.88, and a complementary estimate for the bed material composition of flats. The corresponding values of the geometric mean grain diameter of bars and flats, which range between 2 $1.7 - 26.7\,mm$ and

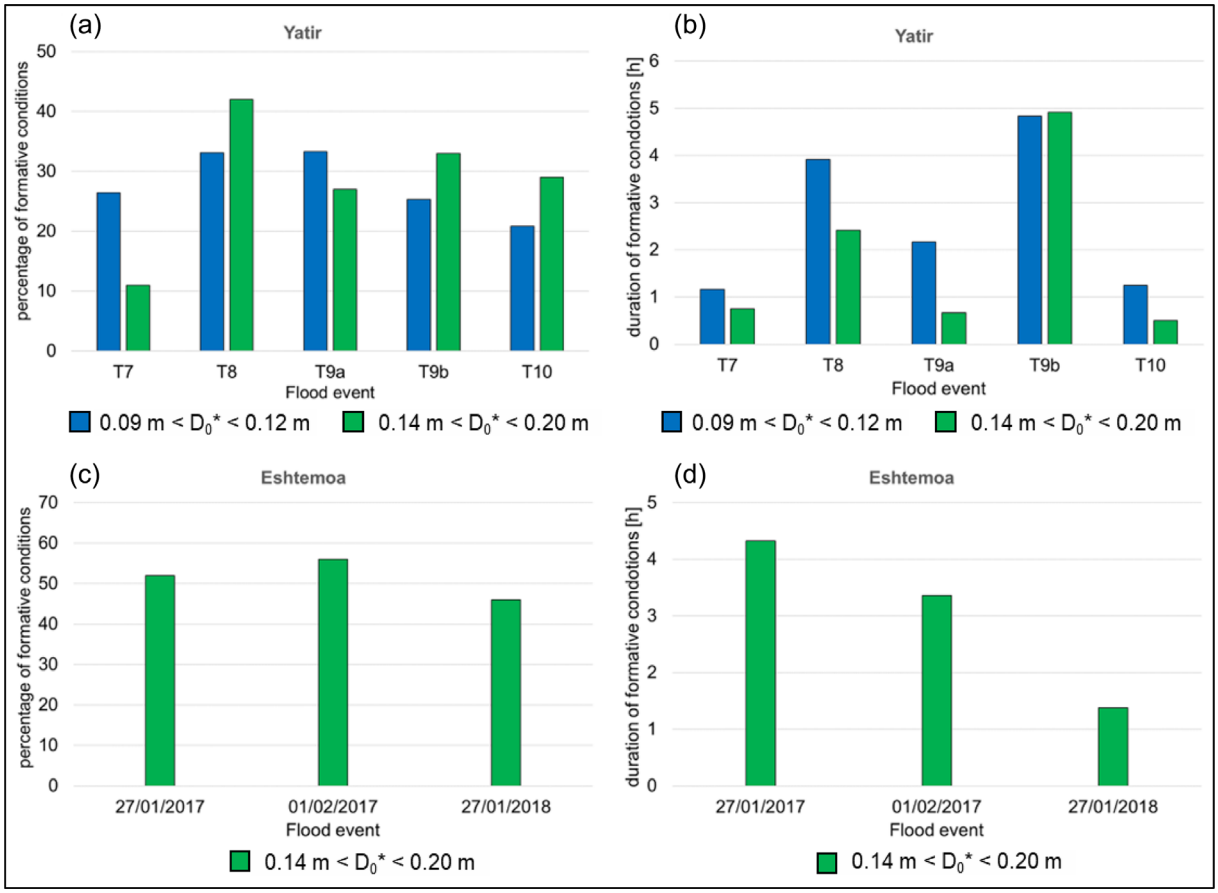

FIGURE 8 The percentage of hydrograph recession duration when the range of formative conditions of bar-flat sequences persists, as predicted by (a and c) linear stability theory and the (b and d) absolute value of such durations, for the flood events in Nahal Yatir and Nahal Eshtemoa reported in Figures 4 and 5, respectively. In the case of Nahal Yatir, blue and green bars refer to the ranges of water depths (D_0^*) obtained with different estimates of the critical depth D_{0c}^*.

4.5 – 5.6 mm, respectively, are consistent with those observed in the Nahal Yatir ($D_{g,\text{bars}} = 25.4$ mm, $D_{g,\text{flats}} = 5.5$ mm) reported in Table 1.

5 | DISCUSSION

The results presented in Section 4 suggest that a linear stability analysis based on a 1-D model for the flow field and the transport of sediment mixtures is capable of predicting the formation of longitudinal, alternating sequences of steep, coarse-grained bars and near-horizontal, fine-grained flats that are observed in ephemeral channels. Their occurrence is driven by a free instability mechanism that reflects the different mobilities of grain sizes in the mixture. The mechanism is promoted when the standard deviation of the sediment mixture is sufficiently large, that is, above an approximate threshold value in the range 1.4 – 1.5, and the Shields stress is not far from the critical threshold for bedload transport. By increasing the Shields stress, the flat-bed configuration turns out to be stable because the difference in grain mobility diminishes as the asymptotic condition of equal mobility is progressively met.

Various approximations have been included in the theoretical analysis to make the problem manageable through an analytical procedure. A simple bi-modal mixture composed of two discrete sizes has been used to represent the GSD. Moreover, the solution has been computed for fixed, albeit different, reach-averaged flow conditions, thus neglecting the effect of flow unsteadiness that may be quite relevant to the short-lived hydrographs typical of dryland channels. Furthermore, the linear solution assumes a regular, periodic longitudinal variation of bed elevation and bed material composition, while the spacing of bars and flats observed in the reach chosen for the field experiment appears irregular (see Laronne et al., 2025, Figure 10). Images of other adjacent reaches of the Nahal Yatir clearly show a more regular spacing (see Powell et al., 2012, Figure 2a, and Reid, Laronne, & Powell, 1995, Figure 3). The irregular spacing may also reflect the effect on bar-flat stability and spacing of width variations that are peculiar to that reach and are controlled, in part, by protruding, dense, woody bank vegetation. In this respect, several theoretical results and experimental evidence have highlighted the control exerted by channel width changes on the development of sedimentary patterns, such as riffle/pool sequences (Morgan & Nelson, 2021; Nelson, Brew, & Morgan, 2015) and the transition of migrating alternate bars to steady central bars (Repetto & Tubino, 1999). The analysis presented here is restricted to a constant-width channel, although it could be readily extended to account for width variations, following the linearised approach proposed by Repetto, Tubino and Paola (2002).

In spite of these approximations, the theoretical results show a fairly good agreement with findings in the ephemeral channels of the northern Negev and reproduce correctly the characteristic features of the bar-flat sequences that are observed in the field. The model's

premises do not account for the complex flow patterns that complicate bed material entrainment and deposition, such as those induced by pebble or cobble clusters (Reid, Frostick, & Brayshaw, 1992). A future challenge would be to incorporate their impact in the model.

It is worth noting that various sedimentary and planform patterns observed in both ephemeral and perennial gravel-bed rivers have hitherto received a sound interpretation through the application of stability theories (e.g. Seminara, 2010). The instability of the liquid–solid interface may involve either the channel bed surface, leading to the formation of bedforms at different spatial scales (dunes, bars and so forth), or the channel banks, resulting in rhythmic variations of channel curvature and width. Unlike these two cases, where the resulting sedimentary patterns reflect the instability of the boundaries themselves, the occurrence of bar-flat sequences appears inherently associated with the spatial arrangement of distinctly different GSDs.

In the case of fluvial bars (or dunes), the instability arises because bedforms drive perturbations of the bed stress and of sediment flux, which in turn enhance the growth of the bedforms, while sediment heterogeneity plays a secondary, opposing role. For instance, field and laboratory observations and theoretical results (Lanzoni & Tubino, 1999; Lisle, Ikeda, & Iseya, 1991; Lisle & Madej, 1992) suggest that bar instability is dampened as the standard deviation of the bed material GSD increases, while the unequal response of different grain sizes to spatial variations of bed stress promotes the occurrence of sorting patterns, the coarser particles accumulating at bar crests and the finer particles accumulating within pools. In this case, the perturbation of the GSD is mainly driven by the perturbation of bed topography.

The present 1-D analysis suggests a different scenario for bar-flat patterns. Instability manifests itself as the growth of a longitudinal perturbation of the spatial displacement of grain sizes of a poorly sorted bed mixture. The perturbation of bed material composition drives a variation in bed elevation and, consequently, a sequence of steeper and less steep segments, which would otherwise not develop spontaneously. A similar mechanism has been introduced to explain the occurrence of fine-grained bedload sheets (Recking et al., 2009; Seminara, Colombini, and Parker, 1996; Whiting et al., 1988), although, in this case, the perturbation of bed elevation vanishes.

Based on the formulation of the problem presented in Section 3, the role of sediment size heterogeneity in the linear solution is twofold. First, bed roughness depends on the local average grain size (see Equation 7). Hence, a perturbation of local bed composition implies a variation of bottom stress. Second, the bedload transport function depends on the reduced hiding function g_{hr} (see Equation 12) that accounts for the effect of the different mobilities of grain sizes in the bed material.

The former effect has been found to play a crucial role in determining bedload sheet instability (Seminara, Colombini, & Parker, 1996), while it is almost negligible in the case of bar-flat sequences. Our sensitivity analysis demonstrates that the boundaries of the instability region do not change appreciably by setting either variable or constant roughness (Figure 9b). Therefore, bar-flat instability appears to be mainly driven by the selective transport of grain sizes because of their different mobilities within the mixture, the effect of which depends on the exponent b of the reduced hiding function g_{hr}. The lower the value of b, the narrower is the instability region (Figure 9a). Results presented in Section 5 have been obtained using the value ($b = 0.26$) calibrated on the ephemeral channels of northern Negev (Powell, Laronne, & Reid, 2003; Powell, Reid, & Laronne, 2001).

The analysis presented herein may shed some light on the conditions that determine the occurrence of alternating bars and flats in ephemeral channels. In general terms, although different sedimentary patterns may also coexist, the occurrence of a dominant mode of instability is more likely to hinder other forms of instability. For instance, one may expect the sorting pattern to be constrained by the stress distribution associated with bed topography when large-scale alternating or point bars are present, as is often the case of perennial gravel-bed streams.

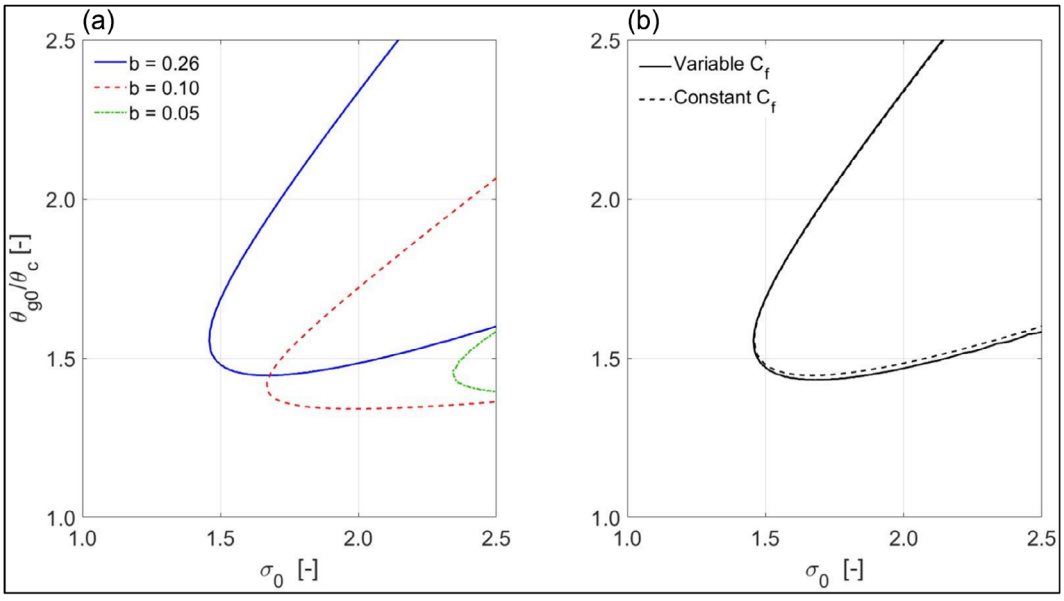

FIGURE 9 Effects of the (a) hiding coefficient b and of the (b) variability of the roughness coefficient C_f on the marginal curves delimiting the instability region for bar-flat patterns. The curves are obtained with $d_{g0} = 0.05$ and $\alpha = 0.02$.

The four channels of the northern Negev desert examined here are characterised by narrow width, very low sinuosity and poorly sorted bed material. Therefore, their aspect ratio is relatively small, and the standard deviation of the bed material GSD is large. According to previous studies (e.g. Colombini, Seminara, & Tubino, 1987; Lanzoni & Tubino, 1999), these are not the most favourable conditions for the formation of large-scale bars, which, on the contrary, develop in much wider channels of the northern Negev (Storz-Peretz et al., 2016; Storz-Peretz & Laronne, 2018), where bar-flat sequences are not observed.

Furthermore, the very short-lived hydrographs typical of these ephemeral channels, which exhibit a rapid rise in water levels and a more gradual recession, may provide favourable conditions for the occurrence of flat-bar patterns. In perennial streams, flats hardly exist and large-scale bars are often very poor in fine-grained sediment (although they may include some fine-grained patches), presumably because the hydrograph recession is sufficiently extended such that most of the fines are moved to pools or to other areas of the bed such as side channels.

Finally, the high sensitivity of the model with respect to the value of the standard deviation of the bed material GSD underlines the need for a sampling technique that effectively includes the finest fraction (down to 2 mm). For the Nahal Yatir, Anim and Cryote, the dataset (Powell et al., 2012) used for modelling incorporates finer grains for the flats than that reported in the companion paper (Laronne et al., 2025) and, therefore, has a higher value of the standard deviation.

6 | CONCLUSIONS

In this study, we have developed a linear stability analysis based on a 1-D model for the flow field and the transport of a sediment mixture to provide a possible explanation for the formation of repeating bar-flat sequences in ephemeral channels of the northern Negev, Israel, and in other channels having comparable hydrological regimes.

The theoretical results show that the occurrence of longitudinal sequences of steep, coarse-grained bars and near-horizontal, fine-grained flats may result from an instability mechanism driven by the different mobilities of grain sizes within the bed material, provided the standard deviation of the sediment mixture exceeds a threshold value and the Shields stress is not far above the critical threshold for bedload transport.

The four channels of the northern Negev desert examined exhibit a value of the standard deviation of bed material GSD that is well above the threshold. Moreover, application of the results of the model demonstrates that conditions that are suitable for bar-flat formation can last several hours during the recession typical of the flood hydrograph of these ephemeral streams. Despite various approximations used in the model, the theoretical results show good agreement with the field observations reported in our companion paper (Laronne et al., 2025) and provide an estimate of the relative importance of the variations of local bed material composition and local bed elevation, as measured in the field.

It is argued that several factors, namely channel geometry (i.e. low sinuosity, narrow width), poorly sorted bed material, and short-lived hydrographs with gradual recession typical of these channels, are likely to create favourable conditions for the generation of repeating bar-flat patterns that are strikingly visible on the dry riverbed after the passage of a flash flood.

NOMENCLATURE

b	Hiding coefficient [−]
C_f	Friction coefficient [−]
D	Water depth [m]
D_g	Geometric mean diameter of the sediment mixture [m]
D_s	Sediment diameter [m]
f	Grain size distribution [−]
Fr	Froude number [−]
$G(\zeta)$	Transport capacity function [−]
g_{hr}	Reduced hiding function [−]
k_s	Roughness height [m]
L_a	Thickness of the active surface layer [m]
p	Sediment porosity [−]
q_s	volume of bedload transport rate per unit width [m]
S	Bed slope [−]
t	Time coordinate [s]
U	Water velocity [m/s]
u_*	Friction velocity [−]
x	Space streamwise coordinate [m]
α	Dimensionless wavenumber of the perturbations [−]
Δ	Relative sediment density [−]
δ	Dirac function [−]
ϵ	Parameter of the small perturbation [−]
ζ	Dummy variable of the transport capacity function [−]
η	Bed elevation [m]
θ_g	Shields parameter associated with the geometric mean diameter [−]
θ_c	Critical Shields parameter [−]
ϕ	Sedimentological, base-2 logarithmic scale for particle size [−]
ρ	Water density [kg/m^3]
ρ_s	Sediment density [kg/m^3]
σ_g	Geometric standard deviation of the grain size distribution [−]
σ	Standard deviation of the grain size distribution [−]
Ψ	Complex coefficients [−]
Ω	Growth rate of perturbations [−]
ω	Angular frequency of perturbations [−]

ACKNOWLEDGEMENTS

We thank Luca Mao, the Review Editor, and the two anonymous reviewers for their insightful and constructive comments, which have enabled us to improve the manuscript. A. Siviglia and M. Tubino acknowledge the Italian Ministry of Education, Universities and Research (MUR) for funding project DICAM-EXC (Departments of Excellence 2023-2027, grant L232/2016), which facilitated their participation in this collaborative research. The project was funded in part by the Israel Science Foundation Grant 832/14. Open access publishing facilitated by Universita degli Studi di Trento, as part of the Wiley - CRUI-CARE agreement.

DATA AVAILABILITY STATEMENT

The data that support the findings of this study are available from the corresponding author upon reasonable request.

ORCID

Gabriele Massera https://orcid.org/0009-0003-0672-1239
Annunziato Siviglia https://orcid.org/0000-0003-1192-1596
Jonathan B. Laronne https://orcid.org/0000-0002-2889-9316
Ian Reid https://orcid.org/0000-0002-8589-0940
D. Mark Powell https://orcid.org/0000-0002-7667-6272
Michael Dorman https://orcid.org/0000-0001-6450-8047
Marco Tubino https://orcid.org/0000-0001-7298-7818

REFERENCES

Callander, R.A. (1969) Instability and river channels. *Journal of Fluid Mechanics*, 36(3), 465–480. Available from: https://doi.org/10.1017/S0022112069001765

Carlin, M., Redolfi, M. & Tubino, M. (2021) The long-term response of alternate bars to the hydrological regime. *Water Resources Research*, 57(7), e2020WR029314. Available from: https://doi.org/10.1029/2020WR029314

Chin, A. & Wohl, E. (2005) Toward a theory for step pools in stream channels. *Progress in Physical Geography: Earth and Environment*, 29(3), 275–296. Available from: https://doi.org/10.1191/0309133305pp449ra

Church, M. & Zimmermann, A. (2007) Form and stability of step-pool channels: research progress. *Water Resources Research*, 43(3), W03415. Available from: https://doi.org/10.1029/2006WR005037

Cohen, T. (2019) The formation of alternate gravel bars with intervening fine-grained flats in desert ephemeral channels exemplified by Nahal Yatir. MSc thesis, Ben Gurion University of the Negev, Department of Geography and Environmental Sciences (in Hebrew with English captions of figures, tables and abstract).

Colombini, M. & Carbonari, C. (2020) Sorting and bed waves in unidirectional shallow-water flows. *Journal of Fluid Mechanics*, 885, A46. Available from: https://doi.org/10.1017/jfm.2019.1039

Colombini, M., Seminara, G. & Tubino, M. (1987) Finite-amplitude alternate bars. *Journal of Fluid Mechanics*, 181, 213–232. Available from: https://doi.org/10.1017/S0022112087002064

Curran, J.C. (2007) Step–pool formation models and associated step spacing. *Earth Surface Processes and Landforms*, 32(11), 1611–1627. Available from: https://doi.org/10.1002/esp.1589

Engelund, F. (1970) Instability of erodible beds. *Journal of Fluid Mechanics*, 42(2), 225–244. Available from: https://doi.org/10.1017/S0022112070001210

Golly, A., Turowski, J.M., Badoux, A. & Hovius, N. (2019) Testing models of step formation against observations of channel steps in a steep mountain stream. *Earth Surface Processes and Landforms*, 44(7), 1390–1406. Available from: https://doi.org/10.1002/esp.4582

Hassan, M.A., Egozi, R. & Parker, G. (2006) Experiments on the effect of hydrograph characteristics on vertical grain sorting in gravel bed rivers. *Water Resources Research*, 42, W09408. Available from: https://doi.org/10.1029/2005WR004707

Hassan, M.A., Saletti, M., McDowell, C. & Li, W. (2022) Sediment dynamics and bed stability in step-pool streams: insights from 18 years of field observations. *Water Resources Research*, 59(1), e2022WR032864. Available from: https://doi.org/10.1029/2022WR032864

Hayashi, T. (1970) Formation of dunes and antidunes in open channels. *Journal of the Hydraulics Division*, 96(2), 357–366. Available from: https://doi.org/10.1061/JYCEAJ.0002324

Hirano, M. (1971) River bed degradation with armouring. *Transactions Japan Society Civil Engineers*, 3(2), 194–195. Available from: https://doi.org/10.2208/jscej1969.1971.195_55

Kennedy, J.F. (1963) The mechanics of dunes and antidunes in erodible-bed channels. *Journal of Fluid Mechanics*, 16(4), 521–544. Available from: https://doi.org/10.1017/S0022112063000975

Keulegan, G.H. (1938) *Laws of turbulent flow in open channels*. National Bureau of Standards.

Lanzoni, S. & Tubino, M. (1999) Grain sorting and bar instability. *Journal Fluid Mechanics*, 393, 149–174. Available from: https://doi.org/10.1017/S0022112099005583

Laronne, J.B., Cohen, T., Powell, D.M., Dorman, M., Siviglia, A., Tubino, M. et al. (2025) Formation of repeating bar-flat bedforms in ephemeral gravel bed channels: 1. Field observations. *Earth Surface Processes and Landforms*, submitted.

Laronne, J.B. & Duncan, M.J. (1992) Bedload transport paths and gravel bar formation. In: Billi, P., Hey, R.D., Thorne, C.R. & Tacconi, P. (Eds.) *Dynamics of gravel bed rivers*. Chichester: Wiley, pp. 177–202.

Laronne, J.B. & Reid, I. (1993) Very high rates of bedload sediment transport by ephemeral desert rivers. *Nature*, 366, 148–150. Available from: https://doi.org/10.1038/366148a0

Laronne, J.B., Reid, I., Yitshak, Y. & Frostick, L.E. (1994) The non-layering of gravel streambeds under ephemeral flood regimes. *Journal of Hydrology*, 159(1-4), 353–363. Available from: https://doi.org/10.1016/0022-1694(94)90266-6

Lisle, T.E., Ikeda, H. & Iseya, F. (1991) Formation of stationary alternate bars in a steep channel with mixed size sediment: a flume experiment. *Earth Surface Processes and Landforms*, 16(5), 463–469. Available from: https://doi.org/10.1002/esp.3290160507

Lisle, T.E. & Madej, M.A. (1992) Spatial variation in armouring in a channel with high sediment supply. In: Billi, P., Hey, R.D., Thorne, C.R. & Tacconi, P. (Eds.) *Dynamics of Gravel Bed Rivers*. Chichester: Wiley, pp. 277–291.

Montgomery, D.R. & Buffington, J.M. (1997) Channel-reach morphology in mountain drainage basins. *Geological Society of America Bulletin*, 109(5), 596–611. Available from: https://doi.org/10.1130/0016-7606(1997)

Morgan, J.A. & Nelson, P.A. (2021) Experimental investigation of the morphodynamic response of riffles and pools to unsteady flow and increased sediment supply. *Earth Surface Processes and Landforms*, 46(4), 869–886. Available from: https://doi.org/10.1002/esp.5072

Nelson, P.A., Brew, A.K. & Morgan, J.A. (2015) Morphodynamic response of a variable-width channel to changes in sediment supply. *Water Resources Research*, 51(7), 5717–5734. Available from: https://doi.org/10.1002/2014WR016806

Parker, G. (1976) On the cause and characteristic scales of meandering and braiding in rivers. *Journal of Fluid Mechanics*, 76(3), 457–480. Available from: https://doi.org/10.1017/S0022112076000748

Parker, G. (1979) Hydraulic geometry of active gravel rivers. *Journal of Hydraulic Engineering*, 105(9), 1185–1201. Available from: https://doi.org/10.1061/JYCEAJ.0005275

Parker, G. (1992) Some random notes on grain sorting. In: *Proc. Grain Sorting Seminar, Ascona, Switzerland*, pp. 19–76.

Powell, D.M., Laronne, J.B. & Reid, I. (2003) The dynamics of bedload sediment transport in low-order, upland, ephemeral gravel-bed rivers. *Advances in Environmental Monitoring and Modelling*, 1(2), 1–27. http://www.kcl/ac/uk/advances/

Powell, D.M., Laronne, J.B., Reid, I. & Barzilai, R. (2012) Repeating reach-scale morphology of upland gravel-bed streams in a semi-arid environment. *Earth Surface Processes and Landforms*, 37(7), 741–753. Available from: https://doi.org/10.1002/esp.3199

Powell, D.M., Reid, I. & Laronne, J.B. (2001) Evolution of bedload grain-size distribution with increasing flow strength and the effect of flow duration on the caliber of bedload sediment yield in ephemeral gravel-bed rivers. *Water Resources Research*, 37(5), 1463–1474. Available from: https://doi.org/10.1029/2000WR900342

Recking, A., Frey, P., Paquier, A. & Belleudy, P. (2009) An experimental investigation of mechanisms involved in bed load sheets production and migration. *Journal of Geophysical Research*, 114, F03010. Available from: https://doi.org/10.1029/2008JF000990

Redolfi, M., Carlin, M. & Tubino, M. (2023) The impact of climate change on river alternate bars. *Geophysical Research Letters*, 50(5), e2022GL102072. Available from: https://doi.org/10.1029/2022GL102072

Reid, I., Frostick, L.E. & Brayshaw, A.C. (1992) Microform roughness elements and the selective entrainment and entrapment of particles in gravel-bed rivers. In: Billi, P., Hey, R.D., Thorne, C.R. & Tacconi, P. (Eds.) *Dynamics of Gravel Bed Rivers*. Chichester: Wiley, pp. 253–266.

Reid, I., Laronne, J.B. & Powell, D.M. (1995) The Nahal Yatir bedload database: sediment dynamics in a gravel-bed ephemeral stream. *Earth*

Surface Processes and Landforms, 20(9), 845–857. Available from: https://doi.org/10.1002/esp.3290200910

Reid, I., Laronne, J.B. & Powell, D.M. (1998) Flash-flood and bedload dynamics of desert gravel-bed streams. *Hydrological Processes*, 12(4), 543–557. Available from: https://doi.org/10.1002/(SICI)1099-1085(19980330)12:4<543::AID-HYP593>3.0.CO;2-C

Repetto, R. & Tubino, M. (1999) Transition from migrating alternate bars to steady central bars in channels with variable width. In: *Proceedings of the International Symposium on River, Coastal and Estuarine Morphodynamics, 1*. Madrid: IAHR, pp. 605–614.

Repetto, R., Tubino, M. & Paola, C. (2002) Planimetric instability of channels with variable width. *Journal of Fluid Mechanics*, 457, 79–109. Available from: https://doi.org/10.1017/S0022112001007595

Richards, K.J. (1980) The formation of ripples and dunes on an erodible bed. *Journal of Fluid Mechanics*, 99(3), 597–618. Available from: https://doi.org/10.1017/S002211208000078X

Richardson, K. & Carling, P.A. (2021) Morphology and origin of alluvial step-pools: A synthesis of experimental and field data from formative flows. *Earth-Science Reviews*, 222, 103823. Available from: https://doi.org/10.1016/j.earscirev.2021.103823

Seminara, G. (2010) Fluvial sedimentary patterns. *Annual Review of Fluid Mechanics*, 42(1), 43–66. Available from: https://doi.org/10.1146/annurev-fluid-121108-145612

Seminara, G., Colombini, M. & Parker, G. (1996) Nearly pure sorting waves and the formation of bedload sheets. *Journal of Fluid Mechanics*, 312, 253–278. Available from: https://doi.org/10.1017/S0022112096001991

Stark, K., Cadol, D., Varyu, D. & Laronne, J.B. (2021) Direct, continuous measurements of sediment transport in a flash flood, sand-rich, gravel-bed ephemeral river. *Geomorphology*, 32, 107682. Available from: https://doi.org/10.1016/j.geomorph.2021.107682

Storz-Peretz, Y. & Laronne, J.B. (2018) The morpho-textural signature of large bedforms in gravel bed channels of various patterns. *Hydrological Processes*. Available from: https://doi.org/10.1002/hyp.11437

Storz-Peretz, Y., Laronne, J.B., Surian, N. & Lucia, A. (2016) Flow recession as a driver of the morpho-texture of braided streams. *Earth Surface Processes and Landforms*, 41(6), 754–770. Available from: https://doi.org/10.1002/esp.3861

Whiting, P.J., Dietrich, W.E., Leopold, L.B., Drake, T.G. & Shreve, R.L. (1988) Bedload sheets in heterogeneous sediment. *Geology*, 16(2), 105–108. Available from: https://doi.org/10.1130/0091-7613(1988)016%3C0105:BSIHS%3E2.3.CO;2

Zapico, I., Laronne, J.B., Lucía, A. & Martín-Duque, J.F. (2018) Morpho-textural implications to bedload flux and texture in the sand-gravel ephemeral Poveda Gully. *Geomorphology*, 322, 53–65. Available from: https://doi.org/10.1016/j.geomorph.2018.08.026

How to cite this article: Massera, G., Siviglia, A., Laronne, J.B., Reid, I., Powell, D.M., Cohen, T. et al. (2025) Formation of repeating bar-flat bedforms in ephemeral gravel bed channels: 2. Bridging mathematical modelling and field observations. *Earth Surface Processes and Landforms*, 50(13), e70184. Available from: https://doi.org/10.1002/esp.70184

APPENDIX A: Linearised form of the governing equations

Here we provide a detailed derivation of the linear differential system for the unknown variables (U_1, D_1, η_1, f_1).

On substituting from (14) into the closure relationships (7), (10) and (12) and neglecting higher-order terms, we derive the following expressions for the coefficients appearing in Equation (15):

$$C_{f0} = \left[6 + 2.5\ln\left(\frac{1}{nd_{g0}2^{\sigma_0}}\right)\right]^{-2}, \quad C_{f1} = C_D\left[D_1 + \ln(2)\left(\overline{\phi}_1 - \sigma_1\right)\right], \tag{A1}$$

$$q_{s0} = \theta_{g0}{}^{3/2}\, G(\zeta_0), \quad q_{s1} = (1.5 + G_\zeta)(C_{f1} + 2U_1) + G_\zeta(1-b)\ln(2)\,\overline{\phi}_1, \tag{A2}$$

where

$$C_D = \frac{1}{C_{f0}}\frac{\partial C_f}{\partial D}\bigg|_{1,\sigma_0} = -5\sqrt{C_{f0}}, \quad G_\zeta = \frac{\zeta_0}{G(\zeta_0)}\frac{\partial G}{\partial \zeta}\bigg|_{\zeta_0} = \frac{4.5}{\zeta_0 - 1}, \quad \zeta_0 = \frac{\theta_{g0}}{\theta_c}\, 2^{b(\phi - \overline{\phi}_0)}, \tag{A3}$$

while $\overline{\phi}_1$ and σ_1 denote the linear perturbations of the first and the second moment of the grain size distribution $f(\phi)$.

By further substituting expansion (14) into the governing equations (1–4) and keeping only the $O(\varepsilon)$ terms, we obtain $D_1 = -U_1$ and the following linear differential problem for the unknown variables (U_1, η_1, f_1):

$$\frac{\partial U_1}{\partial x}\left(1 - Fr_0^{-2}\right) + Fr_0^{-2}\frac{\partial \eta_1}{\partial x} + C_{f0}(3U_1 + C_{f1}) = 0, \tag{A4}$$

$$f_0\frac{\partial \eta_1}{\partial t} + L_{a0}\frac{\partial f_1}{\partial t} + q_{s0}\left(\frac{\partial f_1}{\partial x} + f_0\frac{\partial q_{s1}}{\partial x}\right) = 0, \tag{A5}$$

$$\frac{\partial \eta_1}{\partial t} + \int_{-\infty}^{\infty} q_{s0}\frac{\partial f_1}{\partial x}\,d\phi + \int_{-\infty}^{\infty} q_{s0}f_0\frac{\partial q_{s1}}{\partial x}\,d\phi = 0. \tag{A6}$$

where $L_{a0} = nd_{g0}2^{\sigma_0}$.

Finally, using Equation (A6), we can remove the time derivative of η_1 from the sediment mass balance for each size fraction (A5), which takes the following form:

$$L_{a0}\frac{\partial f_1}{\partial t} + q_{s0}\frac{\partial f_1}{\partial x} - f_0\int_{-\infty}^{\infty} q_{s0}\frac{\partial f_1}{\partial x}\,d\phi + f_0\left(q_{s0}\frac{\partial q_{s1}}{\partial x} - \int_{-\infty}^{\infty} q_{s0}f_0\frac{\partial q_{s1}}{\partial x}\,d\phi\right) = 0. \tag{A7}$$

APPENDIX B: Solution of the linear system

We consider a bimodal mixture composed of two discrete sizes, with GSD given by Equation (18). In this case, the linear perturbations of the first and the second moment of the GSD can be expressed in terms of the linear perturbation of the coarse fraction f_{C1} in the following form:

$$\overline{\phi}_1 = -A_1 f_{C1}, \quad \sigma_1 = A_2 f_{C1}, \tag{A8}$$

where the coefficients A_1 and A_2 depend on the parameters of the unperturbed GSD $f_0(\phi)$

$$A_1 = \frac{\sigma_0}{\sqrt{f_{C0}(1 - f_{C0})}}, \quad A_2 = \frac{\sigma_0(1 - 2f_{C0})}{2f_{C0}(1 - f_{C0})}. \tag{A9}$$

On substituting from (16), where $\widehat{f}_1$ is replaced by $\widehat{f}_{C1}$, into the linearised flow Equation (A4) and using (A1) and (A8), we obtain

$$\widehat{U}_1 = -\widehat{D}_1 = a_1\widehat{\eta}_1 + a_2\widehat{f}_{C1}, \tag{A10}$$

where

$$a_1 = \frac{-i\alpha}{Fr_0^2 C_{f0}(3-C_D) - i\alpha\left(1-Fr_0^2\right)}, \quad a_2 = \frac{Fr_0^2 C_{f0} C_D \ln(2)(A_1+A_2)}{Fr_0^2 C_{f0}(3-C_D) - i\alpha\left(1-Fr_0^2\right)}. \tag{A11}$$

On substituting from Equation (A10) into Equation (A2), and recalling that Equation (16) implies a similar structure for the perturbation of bed load function, we obtain:

$$\widehat{q}_{s1} = a_3\widehat{\eta}_1 + a_4\widehat{f}_{C1}, \tag{A12}$$

where

$$a_3 = a_1(1.5+G_\zeta)(2-C_D),$$
$$a_4 = a_2(1.5+G_\zeta)(2-C_D) - \ln(2)[(1.5+G_\zeta)C_D(A_1+A_2) + G_\zeta A_1(1-b)]. \tag{A13}$$

The coefficients a_3 and a_4, like the unperturbed bedload function q_{s0}, depend on the parameter ζ_0, and therefore, their values change by varying the grain size (see Equation A3).

By further substituting Equation (A9) into the mass balance Equation (A7), as computed for the coarse fraction and the overall mass balance equation for the mixture (A6), we derive the system (20) of two linear differential equations that govern the growth of perturbations of bottom elevation and GSD. The coefficients of the system are

$$\begin{aligned}
\Psi_{11} &= \frac{i\alpha}{L_{a0}}[f_{C0}(f_{C0}q_{sC0}a_{4C} + f_{F0}q_{sF0}a_{4F} + q_{sC0} - q_{sF0}) - q_{sC0}(1+f_{C0}a_{4C})],\\
\Psi_{12} &= \frac{i\alpha}{L_{a0}}f_{C0}(f_{C0}q_{sC0}a_{3C} + f_{F0}q_{sF0}a_{3F} - q_{sC0}a_{3C}),\\
\Psi_{21} &= -i\alpha(f_{C0}q_{sC0}a_{4C} + f_{F0}q_{sF0}a_{4F} + q_{sC0} - q_{sF0}),\\
\Psi_{22} &= -i\alpha(f_{C0}q_{sC0}a_{3C} + f_{F0}q_{sF0}a_{3F}),
\end{aligned} \tag{A14}$$

where the subscripts C and F denote the values of the bedload function q_{s0} and of the coefficient a_3 and a_4 corresponding to the coarse-grained and the fine-grained fraction, respectively.